

2020-08-15

Carbonate clumped isotope evidence for latitudinal seawater temperature gradients and the oxygen isotope composition of Early Cretaceous seas

Watanabe, Sayaka

<http://hdl.handle.net/10026.1/15733>

10.1016/j.palaeo.2020.109777

Palaeogeography, Palaeoclimatology, Palaeoecology

Elsevier BV

All content in PEARL is protected by copyright law. Author manuscripts are made available in accordance with publisher policies. Please cite only the published version using the details provided on the item record or document. In the absence of an open licence (e.g. Creative Commons), permissions for further reuse of content should be sought from the publisher or author.

1 **Carbonate clumped isotope evidence for latitudinal seawater temperature gradients and the**
2 **oxygen isotope composition of Early Cretaceous seas**

3

4 Gregory D. Price^{1*}, David Bajnai^{2,3}, Jens Fiebig²

5

6 ¹ School of Geography, Earth & Environmental Sciences, University of Plymouth, Drake Circus,
7 PL4 8AA Plymouth, UK

8 ² Institute of Geosciences, Goethe University Frankfurt, Altenhöferallee 1, 60438 Frankfurt am
9 Main, Germany

10 ³ Institute of Geology and Mineralogy, University of Cologne, Zùlpicher Str. 49b, 50674 Cologne,
11 Germany

12 *Corresponding author, email: g.price@plymouth.ac.uk, phone: +44 1752 584771

13

14 **Keywords:** thermometry, Valanginian, stable isotopes, belemnites

15 **Abstract**

16 In this study, we investigated Early Cretaceous (Valanginian, ca. 135 million years ago)
17 climate from subtropical to boreal palaeolatitudes. Combined carbonate clumped isotope and
18 oxygen isotope data derived from sub-arctic, boreal, and sub-tropical fossil belemnite rostra
19 (Mollusca: Cephalopoda) provide new palaeotemperature estimates as well as a constraint on
20 the oxygen isotope composition of seawater. Our belemnite data reveal balmy high-latitude
21 marine temperatures (ca. 22 °C) and warm sub-tropical temperatures (ca. 31 °C).
22 Supplementing our clumped isotope-based temperature estimates with published TEX₈₆ data
23 results in a conservative reconstruction of a latitudinal temperature gradient that is reduced
24 compared to modern conditions. We find that modelling efforts are close to reproducing
25 tropical temperatures when high $p\text{CO}_2$ levels are considered. Warm polar temperatures imply,
26 however, that data-model discrepancies remain. Early Cretaceous seawater oxygen isotope
27 values show a modern profile and are much more positive (up to 1.5‰ SMOW) than typically
28 assumed. Based on our findings, if the positive Cretaceous seawater $\delta^{18}\text{O}$ values are not
29 considered, carbonate $\delta^{18}\text{O}$ thermometry would underestimate temperatures, most acute at
30 middle and tropical latitudes.

31 **1 Introduction**

32 Existing proxy data suggest that the Cretaceous latitudinal sea-surface temperature
33 (SST) gradient was reduced (Barron, 1983; Naafs and Pancost, 2016; Littler et al., 2011; Voigt et
34 al., 2003; Pucéat et al., 2003). The presence of extensive polar ice at this time, as suggested by
35 Miller (2009) for example, is at odds with contemporaneous warm polar ocean temperatures,
36 variable but high atmospheric CO₂ level (Bernier and Kothavala, 2001; Wang et al., 2014;
37 Witkowski et al., 2018) and the occurrence of tropical flora at mid- to high latitudes (Grasby et
38 al., 2017). During much of the Cretaceous, stable oxygen isotope and TEX₈₆ evidence suggests
39 that equatorial surface waters were warmer (ca. 30–40 °C) and greater than the maximum SSTs
40 recorded in the modern ocean (e.g. O'Brien et al., 2017; Huber et al., 2018). Mid to higher
41 latitude surface waters were also 10–20 °C warmer than today (Naafs and Pancost, 2016; Littler
42 et al., 2011; O'Brien et al., 2017; Huber et al., 1995; Jenkyns et al., 2012; Vickers et al., 2019;
43 O'Connor et al., 2019).

44 The stable oxygen isotope composition ($\delta^{18}\text{O}$) of skeletal marine carbonates is perhaps
45 the most widely used palaeotemperature proxy (Barron, 1983; Voigt et al., 2003; Pucéat et al.,
46 2003; Huber et al., 2018; Mutterlose et al., 2012; Price et al., 2018). The challenge is, however,
47 that the oxygen isotope composition of skeletal carbonates in marine systems vary as a
48 function of both ambient temperatures and the oxygen isotope composition of seawater
49 ($\delta^{18}\text{O}_{\text{sw}}$). Obtaining a value for $\delta^{18}\text{O}_{\text{sw}}$ is complicated because of variables that cannot be easily
50 independently quantified, such as freshwater input, evaporation, and the extent of polar ice
51 (Frakes and Francis, 1988; Price, 1999; Miller, 2009; Wierzbowski et al., 2018). Additionally, a
52 proposed change in the mode of mid-ocean ridge hydrothermal alteration over tens of million
53 year timescales suggests that the $\delta^{18}\text{O}_{\text{sw}}$ value has increased gradually through Earth's history,
54 from ca. -6‰ SMOW in the Cambrian to its present value of ca. 0‰ SMOW (Standard Mean
55 Ocean Water) (Veizer and Prokoph, 2015; Jaffrés et al., 2007). Nevertheless, the implied

56 climatic warmth, derived from the $\delta^{18}\text{O}$ values of skeletal marine carbonates, is consistent with
57 more qualitative data derived from thermophilic floras and faunas from the high latitudes
58 (Frakes and Francis, 1988; Tarduno, et al., 1998; Hurum et al., 2006; Spicer et al., 2008; Spicer
59 and Herman 2010). However, Cretaceous General Circulation Model (GCM) simulations indicate
60 that the latitudinal temperature gradient was much steeper than what the geological record
61 suggests (Donnadieu et al., 2016; Lunt et al., 2016; Zhou et al., 2008; Poulsen et al., 2007).

62 The clumped isotope palaeothermometry technique measures the abundance of heavy
63 (^{13}C – ^{18}O bond bearing, mass 47) carbonate isotopologues within the single carbonate phase
64 relative to its stochastic distribution, which is expressed as the Δ_{47} value. Clumped isotope-
65 derived seawater temperatures are independent of the oxygen isotope composition of the
66 waters (Ghosh et al., 2006). In this study, we analyse belemnite rostra (fossil remains of extinct
67 marine cephalopods) using clumped isotope thermometry to provide new Δ_{47} data from the
68 Early Cretaceous (Valanginian). Further, we examine equator-to-pole seawater temperature
69 gradients and the $\delta^{18}\text{O}_{\text{sw}}$ values to aid temperature reconstructions and palaeoclimate
70 modelling efforts.

71

72 **2 Materials and methods**

73 *2.1 Stratigraphic and environmental setting*

74 Belemnite rostra for this study were collected from four locations: the Khatanga Basin
75 (Boyarka River, Russia, 70.592611° N, 97.369083° E), the Pechora Basin (Izhma River, Russia,
76 64.835150° N, 53.782200° E), the Cleveland Basin (Speeton, UK, 54.160555° N, 0.236111° W),
77 and Caravaca (Southern Spain, 38.086944° N, 1.853889° W). These sites are spread across
78 Tethyan, sub-Boreal, and Boreal locations, with palaeolatitudes ranging from 24° N to 74° N
79 (Fig. 1).

80 The Lower Cretaceous part of the Boyarka River section is ca. 300 m thick and consists
81 of marine sandstones, siltstones, and clays deposited in water depths of less than 100 m (Nunn
82 et al., 2010). The fully marine macrofauna includes belemnites and ammonites, allowing a
83 detailed Valanginian biostratigraphic zonation consistent with the Boreal biostratigraphic
84 schemes (Fig. 2) and correlatable to Tethyan ammonite biostratigraphy (Nunn et al., 2010;
85 Shulgina et al., 1994; Zakharov et al., 1997). Burial-history analysis of the Boyarka River region
86 of the Khatanga Basin, suggests that a maximum burial depth is likely to be ca. 500 m and
87 geothermal gradients to be moderate ca. 40 °C/km (Klett et al., 2011; Dobretsov et al., 2013).

88 The ca. 62-m-thick Izhma River section comprises shallow marine clastics with
89 belemnites and ammonites present throughout. A detailed Berriasian (Ryazanian) to
90 Valanginian biostratigraphic zonation is consistent with the Boreal biostratigraphic schemes
91 and correlatable to Tethyan ammonite biostratigraphy (Nunn et al., 2010; Baraboshkin, 2004;
92 Zakharov et al., 1997). Burial history curves suggest that the burial depth is likely to be no more
93 than 1000 m, and the present thermal gradients in the Pechora Basin are moderate ca. 19–
94 35 °C/km (Lindquist, 1999).

95 The Lower Cretaceous successions located near Caravaca, Southern Spain (Mai Valera,
96 Sierra de Quipar, Canada Luenga) consist of nodular limestones with abundant marine fossils,
97 including crinoid fragments, overlain by hemipelagic marl-limestone alternations (Aguado et al.,
98 2000). The successions are thought to have been deposited in a low-energy marine basinal
99 setting, with an estimated water depth of a few hundreds of meters (Company and Tavera,
100 2015). Here, the macrofauna consists mainly of belemnites and well-preserved ammonites,
101 allowing detailed biostratigraphic zonation and correlation of the sections (Aguado et al., 2000;
102 Janssen, 2003; Company and Tavera, 2015; Price, et al., 2018). The maturity of the organic
103 matter in these Subbetic sections and other diagenetic observations imply that the burial depth

104 was no more than 1000 m and that the sediments never reached more than 80 °C (Reicherter
105 et al., 1996).

106 The Speeton Clay Formation of the Cleveland Basin comprises about 100 m of
107 interbedded shallow marine claystones deposited in water depths of less than 100 m. The
108 stratigraphical succession contains abundant belemnite rostra and well-preserved ammonites,
109 allowing detailed biostratigraphy (Rawson, 1973; McArthur et al., 2004) and correlation to
110 Boreal and Tethyan zonation schemes (Fig. 2). Measured $^{87}\text{Sr}/^{86}\text{Sr}$ values (McArthur et al., 2004)
111 show a good agreement between the biostratigraphic data. Vitrinite reflectance data collected
112 and analysed by Hemingway and Riddler (1982) for the Middle Jurassic, which lies beneath the
113 Speeton Clay Formation provides a temperature value of 95 °C for these Jurassic rocks. Holliday
114 (1999) took this information and assuming an average thermal conductivity provided a
115 geothermal gradient of approximately 30 °C/km and estimated maximum burial depths of ca.
116 2000 m. For the Cretaceous, the estimated sediment surface temperature used was 20 °C
117 (Holliday, 1999). These temperature estimates are consistent with the thermal history model
118 presented by Słowakiewicz et al. (2015) that suggests that the maximum temperatures for the
119 Lower Cretaceous succession reached ca. 40–50 °C during the early Cenozoic.

120 Theoretical calculations based on laboratory experiments evidence that solid-state
121 diffusion, even in wet and high-pressure conditions, is insignificant below 100 °C burial
122 temperatures on a timescale of 135 million years (Passey and Henkes 2012; Brenner et al.,
123 2018). Thus, the belemnite rostra analysed from these four sections should not have been
124 affected by solid-state reordering.

125

126 2.2 *Sample selection*

127 Belemnite rostra consist of diagenetically stable low-Mg calcite (Saelen, 1989). The
128 rostra selected for analysis in this study were those deemed to be the best-preserved samples

129 in the previous studies of McArthur et al. (2004), Nunn et al. (2010), Price et al. (2000), and
130 Price et al. (2018). The excellent preservation of the analysed material is indicated by trace
131 element concentrations and petrographic analyses, including cathodoluminescence. Diagenetic
132 alteration of marine calcites often leads to significant enrichments in Mn and Fe (Veizer, 1974).
133 Diagenetic Mn²⁺ ions are also an activator of orange cathodoluminescence in calcites, which is
134 indicative of the alteration under reducing conditions (Marshall, 1992). All the belemnites
135 analysed for clumped isotopes, in this study, had low concentrations of Fe (< 120 ppm) and Mn
136 (< 25 ppm) indicative of good sample preservation (e.g. McArthur et al., 2007; Mutterlose et al.,
137 2012). These 20 Valanginian belemnite rostra were: *Acroteuthis* sp. from Speeton from the
138 Polyptychites Ammonite zone; *Berriasibelus*, *Hibolithes* and *Duvalia* from Caravaca from the
139 Pertransiens–Verrucosum Ammonite zones; *Acroteuthis* and *Pachyteuthis* from Pechora Basin
140 from the Klimovskiensis to Michalskii Ammonite zones, and *Acroteuthis*, *Lagonibelus* and
141 *Pachyteuthis* from Khatanga Basin from the Klimovskiensis to Michalskii Ammonite zones
142 schemes (Fig. 2). Calcite subsamples (ca. 50 mg carbonate powder) were taken from previously
143 investigated rostra (see above), re-sampled across multiple growth bands, in order to get a
144 representative amount for clumped isotope analysis. During sampling the belemnite rostra
145 margins and calcite around the apical zones were avoided, as diagenetic alteration is typically
146 observed in these parts. Visual inspection also showed belemnite rostra preservation to be
147 excellent with all specimen displaying honey coloured translucent calcite. This is consistent with
148 petrographic and cathodoluminescence observations (e.g. non-luminescent rostra) made in
149 previous research (McArthur et al., 2004; Nunn et al., 2010; Price et al., 2000, 2018).

150

151 2.3 Clumped and stable isotope analyses

152 Clumped isotope analyses were performed using a ThermoFisher MAT 253 gas-source
153 isotope-ratio mass spectrometer connected to an automated gas extraction and purification

154 line at the Institute of Geosciences, Goethe University Frankfurt. Carbonates were digested at
155 90 °C in a common acid bath. Background correction for the clumped isotope analyses was
156 performed as described in Fiebig et al. (2016). Raw isotope values were calculated using the
157 [Brand]/IUPAC set of isotopic parameters as suggested by Daëron et al. (2016). The raw Δ_{47}
158 data were projected to the carbon dioxide equilibrium scale using empirical transfer functions
159 that were determined using equilibrated gases (25 °C and 1000 °C, respectively) of various bulk
160 isotope composition (Petersen et al., 2019). A 90–25 °C acid fractionation factor of 0.088‰ was
161 applied to all $\Delta_{47(RFAC)}$ values (Petersen et al., 2019). To verify the consistency and precision of
162 the clumped isotope measurements six carbonate standards were independently analysed
163 along with the samples. The $\Delta_{47(RFAC)}$ (1 standard deviation, N = number of replicates) values of
164 the reference material are: Carrara 0.407‰ (0.019‰, N = 335), MuStd 0.749‰ (0.018‰, N =
165 181), ETH 1 0.301‰ (0.016‰, N = 78), ETH 2 0.301‰ (0.019‰, N = 37), ETH 3 0.711‰
166 (0.018‰, N = 92), ETH 4 0.556‰ (0.020‰, N = 10) (Data S1). To convert $\Delta_{47(RFAC)}$ values to
167 temperatures, we used a synthetic calcite calibration: $\Delta_{47(RFAC)} = 0.0383(\pm 1.7E-06) \times 10^6/T^2 +$
168 $0.258(\pm 1.7E-05)$ (Petersen et al., 2019), where T is in K and $\Delta_{47(RFAC)}$ is in ‰. $\delta^{18}O_{sw}$ estimates
169 (Table 1, Data S1) were calculated using the Δ_{47} -derived temperature, the measured $\delta^{18}O$ value
170 of each belemnite, and the $1000 \ln \alpha_{\text{calcite-water-temperature}}$ relationships of Kim and O’Neil
171 (1997) (corrected for a CO₂-calcite acid fractionation factor of 10.25, Kim et al. (2007)) and of
172 Coplen (2007). Coplen (2007) provided an equation based on water and vein calcite
173 precipitated at extreme slow rates subaqueously at Devils Hole, Nevada, USA. The widely
174 accepted Kim and O’Neil (1997) equation is based on inorganic precipitation experiments.

175

176 **3 Results**

177 *3.1 Belemnite Δ_{47} -based temperatures*

178 The average Δ_{47} -derived temperatures of this study range from 19 °C to 27 °C (Fig. 3,
179 Table 2, Supplementary Figure 1, Data S1). Some studies have postulated that belemnites
180 calcified their rostra, possibly seasonally, in the upper part of the water column (Klug et al.,
181 2016; Price et al., 2015; Stevens et al., 2014), whereas others consider belemnites as
182 nektobenthic organisms (Wierzbowski et al., 2013). For shallow marine settings (i.e. typically
183 less than 100 m), comparable to the locations investigated in this study (see above), one could
184 assume a low temperature gradient in the water column. Thus, here we presume that
185 belemnites indicate mean seawater temperatures at these sites at the time of rostra growth.
186 The range of Δ_{47} -derived temperatures encountered at each of the individual sample site was
187 from 4 °C to 15 °C. This relatively large temperature range is similar to that seen in other
188 clumped isotope studies (e.g. Petersen et al., 2016; Evans et al., 2018; Meyer et al., 2018). Such
189 a range in the Δ_{47} -derived temperature data is of a similar magnitude as the modern
190 temperature range (e.g. 4–12 °C) in similar latitudes (Locarnini et al., 2013) and is attributed to
191 a combination of the influence of seasonal temperature variability, different belemnite
192 ecologies combined with the impact of local geography and a reflection of the range of
193 temperature variability over the timescales represented by the belemnite sample set (see Fig.
194 2).

195 Our Δ_{47} -derived temperature estimate for the Valanginian low latitudes (27 °C) is lower
196 than the average temperature values of ca. 35 °C obtained from Valanginian $\text{TEX}_{86}^{\text{H}}$ data (Littler
197 et al., 2011) but is comparable with modern mean annual surface temperature observations.
198 Our Δ_{47} -based temperatures suggest, therefore, that belemnites were calcifying their rostra in
199 waters slightly cooler than those surface waters indicated by the TEX_{86} data. Notably, the
200 belemnites from Caravaca occur in hemipelagic marly-limestone beds formed at a depth of a
201 few hundred meters (see above) and may have lived at times below a thermocline layer, so
202 their clumped isotope record may be subject to lower temperatures. Vickers et al. (2019) also

203 showed that Δ_{47} -derived palaeotemperatures were slightly cooler than TEX_{86} -based estimates.
204 Multiple studies have now found that clumped temperatures of molluscs are always colder
205 than TEX_{86} , temperature estimates, whether using the $\text{TEX}_{86}^{\text{H}}$ or BAYSPAR TEX_{86} calibration. The
206 temperature difference is commonly too great to be explained by surface vs. benthic modes of
207 life alone (see Meyers et al., 2018). Despite the relatively large uncertainty in our temperatures
208 estimates, our average Valanginian temperatures (19–24 °C) for the middle latitudes are
209 warmer by up to 13 °C than other Valanginian temperature estimates derived from $\delta^{18}\text{O}$
210 thermometry of belemnites (Schootbrugge et al., 2000; Price et al., 2000; McArthur et al.,
211 2004), although similar to Pucéat et al. (2003), who inferred temperatures from the oxygen
212 isotope composition of fish tooth enamels. Our average Valanginian temperatures are also
213 comparable to $\text{TEX}_{86}^{\text{H}}$ data from other Cretaceous intervals (Mutterlose et al., 2010, 2012;
214 Naafs and Pancost, 2016; O'Brien et al., 2017). For example, Mutterlose et al. (2012) suggest
215 $\text{TEX}_{86}^{\text{H}}$ seawater temperature estimates ranging from 22 °C to 24 °C for the Hauterivian of
216 Speeton, UK. The temperature estimate for higher paleolatitudes (74° N) from this study is
217 19 °C and is warmer than previous Valanginian carbonate $\delta^{18}\text{O}$ -based estimates (Price and
218 Nunn, 2010; Ditchfield, 1997) but similar to Late Cretaceous $\text{TEX}_{86}^{\text{H}}$ seawater temperature
219 estimates (Super et al., 2018). Different calibrations have been proposed to translate TEX_{86} into
220 SST. Of these calibrations, the global nonlinear logarithmic $\text{TEX}_{86}^{\text{H}}$ calibration of Kim et al.
221 (2010) and the BAYSPAR TEX_{86} calibration of Tierney and Tingley (2014) are the most commonly
222 chosen for higher-temperature settings, such as in the Cretaceous. It is the more conservative
223 $\text{TEX}_{86}^{\text{H}}$ estimates that provide a better match to our clumped isotope temperature estimates
224 (see also Vickers et al., 2019). The BAYSPAR TEX_{86} calibration of Tierney and Tingley (2014)
225 provides higher temperatures (ca. 8 °C higher) at the upper limit of the proxy (e.g. O'Brien et al.
226 2017; O'Connor et al., 2019). Our Valanginian seawater temperatures across all latitudes are

227 also 1–14 °C warmer than modern SST observations, although at middle latitudes, they
228 approach the warmest recent observations (Locarnini et al., 2013).

229 The interpretation of relatively warm past ocean temperatures at middle-high latitudes
230 is consistent with palaeobotanical temperature constraints derived from Cretaceous fossil
231 floras (Spicer and Herman, 2010). In contrast, data from the Lower Cretaceous of Canada
232 (Grasby et al., 2017), Svalbard (Vickers et al., 2016), and Siberia (Rogov et al., 2017) suggest that
233 numerous boreal cool events interrupted otherwise warm conditions. These authors describe
234 abundant glendonites (pseudomorphs after marine sedimentary ikaite) in Valanginian and
235 Aptian strata that are thought to be critical markers of cold conditions. These observations are
236 not incompatible with our data from the Valanginian, as Grasby et al. (2017) conclude that cold
237 periods were brief, punctuating an overall warm Early Cretaceous climate.

238

239 **4 Discussion**

240 *4.1 Early Cretaceous latitudinal temperature gradient*

241 Using the average palaeotemperatures and the palaeolatitude (Young et al., 2019) at
242 each of the sites examined here, together with Valanginian Δ_{47} data from Price and Passey
243 (2013) and TEX₈₆ data from Littler et al. (2011), we can conservatively reconstruct an Early
244 Cretaceous latitudinal temperature profile with an estimated gradient of ca. 0.32 °C per degree
245 of latitude, between 15° N and 74° N (Fig. 3). TEX₈₆ data from other Early Cretaceous intervals
246 (Naafs and Pancost, 2016) and Late Cretaceous $\delta^{18}\text{O}$ -derived palaeotemperatures (Voigt et al.,
247 2003; Pucéat et al., 2003) also reveal a similar gradient. Available TEX₈₆ data evidence (O’Brien
248 et al. 2017; O’Connor et al., 2019) suggests that latitudinal temperature gradients were lower in
249 the Coniacian to Campanian compared with the present day. The implied shallow meridional
250 temperature gradient for the Early Cretaceous contrasts with a modern average gradient of ca.
251 0.45 °C per degree of latitude in the Northern Hemisphere (Young et al., 2019).

252 Most evidence suggests that the Cretaceous was characterised by high atmospheric CO₂
253 levels (e.g. Berner and Kothavala, 2001; Wang et al., 2014; Witkowski et al., 2018) and
254 consequently, its climate was warmer and more equable (Frakes 1979; Huber et al., 1995; Bice
255 et al., 2003). Although, as noted above, transient cool events have been suggested (Grasby et
256 al., 2017; Mutterlose et al., 2010; McArthur et al., 2007), data typically point to warm polar
257 regions (Spicer and Herman, 2010; Ditchfield 1997; Frakes, 1979; McArthur et al., 2007)
258 consistent with our temperature estimates. The presence of such a reduced temperature
259 gradient requires a climate mechanism in a high *p*CO₂-world that yields temperate polar regions
260 while not overheating the tropics. Proposed mechanisms to increase the transfer of heat
261 toward the poles include increased oceanic (Schmidt and Mysak, 1996) and atmospheric
262 poleward heat transport (Bice et al., 2003), together with amplification of polar warmth by
263 cloud feedbacks (Kump and Pollard 2008; Sagoo et al., 2013; Upchurch et al., 2015).

264

265 4.2 *Cretaceous model-data comparisons*

266 Climate modelling of past warm periods has received much attention as it has long been
267 suggested that simulations may not capture the extent to which the latitudinal temperature
268 gradient is reduced (Spicer, et al., 2008). The Δ_{47} reconstructions and temperature compilation
269 demonstrate that Early Cretaceous tropical warming was of a magnitude consistent with some
270 models (e.g. using the fast ocean atmosphere model (FOAM), for the Late Cretaceous,
271 Donnadieu et al., 2016) at 12-times pre-industrial *p*CO₂ (Fig. 3). Other simulations indicate
272 cooler tropical temperatures. For example, modelled Valanginian sea surface temperatures
273 (using the UK Met Office HadCM3L model) with 4x pre-industrial *p*CO₂ (Lunt et al., 2016) shows
274 less of a fit particularly with the Littler et al. (2011) TEX₈₆ temperature data, which represents
275 the sea surface, as does the model. For higher latitudes, our temperature proxy data are
276 warmer than some simulations (Donnadieu et al., 2016; Lunt et al., 2016; Poulsen et al., 2007;

277 Upchurch et al., 2015) for the Early and Late Cretaceous even at 12-times pre-industrial $p\text{CO}_2$.
278 In contrast to these Cretaceous simulations, climate models of other “greenhouse” intervals
279 (e.g. for the Eocene, Sagoo et al., 2013; Zhu et al., 2019), show warmer higher latitudes.
280 Although many aspects contributed to the warmth seen at higher latitudes in the model of
281 Sagoo et al., (2013), a strong sensitivity to albedo changes associated with cloud cover was
282 apparent. However, for the highest latitude proxy data, the magnitude of warming simulated
283 by most climate models is still less than indicated by the Δ_{47} data and published TEX_{86} (Jenkyns
284 et al., 2012) temperature estimates. This could suggest that some climate models for the
285 Cretaceous are still missing key processes. Notably, Upchurch et al. (2015) using a fully coupled
286 GCM come close to reproduce warm Cretaceous polar temperatures and the latitudinal
287 temperature gradient without overheating the tropics. For a cool greenhouse interval of the
288 latest Cretaceous (Maastrichtian) the best fits of Upchurch et al. (2015) for mean annual
289 temperature are simulations that use 6-times pre-industrial levels of atmospheric CO_2 , or 2-
290 times pre-industrial levels of atmospheric CO_2 and liquid cloud properties that may reflect pre-
291 anthropogenic levels of cloud condensation nuclei. It is important to note that Cretaceous TEX_{86}
292 data and Δ_{47} -derived temperatures are limited by the distribution of suitably preserved
293 sediments at high latitudes. Indeed, Cretaceous TEX_{86} data is available from just a few Arctic
294 sites (Jenkyns et al., 2004; Super et al., 2018). As such, the high temperatures so far identified
295 may not be fully representative of regional averages.

296

297 *4.3 The oxygen isotope composition of Early Cretaceous seas*

298 Estimations of ancient oceans $\delta^{18}\text{O}_{\text{sw}}$ values are controversial. Complexity arises from
299 variables such as the input of freshwater and evaporation, the presence or absence of polar ice,
300 whether the oxygen isotope composition of the seawater is buffered by submarine
301 hydrothermal processes, or whether lower $\delta^{18}\text{O}$ values of ancient marine carbonates reflect the

302 fact that the $\delta^{18}\text{O}_{\text{sw}}$ value has varied significantly over time (see Jaffrés et al., 2007). The
303 average of our $\delta^{18}\text{O}_{\text{sw}}$ estimates is calculated as -0.1‰ SMOW using the Coplen (2007) equation
304 or 1.4‰ SMOW using the Kim and O’Neil (1997) equation (Table 2, Data S1). Both values are
305 more positive than the estimated global average $\delta^{18}\text{O}_{\text{sw}}$ value for the modern ocean (-0.28‰
306 SMOW) or an ice-free world (-1.0‰ SMOW) (Shackleton and Kennett, 1975) (Fig. 4). The $\delta^{18}\text{O}_{\text{sw}}$
307 value of -1.0‰ SMOW is widely cited as the mean seawater oxygen isotope composition for the
308 Cretaceous. Nevertheless, our data from four new sites, in conjunction with data from Price
309 and Passey (2013), suggests a gentle decrease in average values poleward (Fig. 4,
310 Supplementary Figure 2) (see also Zhou et al., 2008). The difference between our calculated
311 $\delta^{18}\text{O}_{\text{sw}}$ values and modern $\delta^{18}\text{O}_{\text{sw}}$ values, or the assumed $\delta^{18}\text{O}_{\text{sw}}$ values for ancient seas in ice-
312 free hothouse worlds, may be due to (1) differences in the absolute Δ_{47} -temperature calibration
313 producing temperatures that are too warm, (2) vital effects in the belemnites resulting in
314 carbonate $\delta^{18}\text{O}$ values enriched relative to equilibrium with seawater, (3) diagenesis causing
315 lower Δ_{47} and higher $\delta^{18}\text{O}$ values in carbonates, or (4) changes in $\delta^{18}\text{O}_{\text{sw}}$ values of ancient seas.

316 Differences in the Δ_{47} -temperature calibration would influence absolute temperature
317 and calculated $\delta^{18}\text{O}_{\text{sw}}$ values. As noted above, we used the synthetic Δ_{47} -temperature
318 calibration of Petersen et al. (2019) to convert the measured clumped isotope values to
319 precipitation temperatures of calcium carbonate. This calibration is fairly robust as it considers
320 451 carbonate datapoints. In comparison, the in-house Wacker et al. (2014) or the steeper
321 sloped Kelson et al. (2017) calibrations give temperatures that are ca. 3 °C warmer (Data S1).
322 Hence our choice of calibration eliminates potential biasing towards too warm temperatures.

323 Alternatively, the high $\delta^{18}\text{O}_{\text{sw}}$ values could be caused by diagenetic effects that
324 increased temperatures. Modelling of burial at all sites suggests that the belemnite rostra
325 analysed should not have been affected by solid-state reordering. Alternatively, the high $\delta^{18}\text{O}_{\text{sw}}$
326 values may be due to vital effects. Should Kim and O’Neil (1997) represent equilibrium, then

327 our mean $\delta^{18}\text{O}_{\text{sw}}$ value would be on average 2.4‰ higher than the value assumed for an ice-
328 free ocean (see below). Kinetic isotope effects generally, however, discriminate against the
329 heavier isotope (e.g. McConnaughey 1989), although Price et al. (2015) do suggest a possible
330 offset between belemnite calcite $\delta^{18}\text{O}$ and equilibrium of ca. 1‰. Data from a number of other
331 Cretaceous studies applying the clumped isotope palaeothermometer to molluscs (Dennis et
332 al., 2013; Meyer et al., 2018; Vickers et al., 2019), also indicates that the isotopic composition
333 of seawater predicted was markedly positive, using the equation of Kim and O'Neil (1997) and
334 exceeding modern seawater values. Further work comparing the clumped isotope
335 temperatures to different molluscs (see Meyer et al. 2018) could resolve whether these high
336 $\delta^{18}\text{O}_{\text{sw}}$ values could be caused by vital effects.

337 In addition to those studies noted above, data from a number of other studies applying
338 the clumped isotope palaeothermometer (Petersen and Schrag 2015; Wierzbowski et al 2018),
339 also note that the isotopic composition of seawater predicted was, at times, markedly positive.
340 This poses a challenge, as the average value of modern $\delta^{18}\text{O}_{\text{sw}}$ is a consequence of ice
341 accumulation largely on Greenland and Antarctica. Although modest-sized Cretaceous ice
342 sheets have been postulated (DeConto and Pollard, 2003; Frakes and Francis, 1988; Price,
343 1999), the volume of this ice is likely to be insufficient to see $\delta^{18}\text{O}_{\text{sw}}$ values around 1‰ SMOW.
344 $\delta^{18}\text{O}_{\text{sw}}$ values of 1‰ SMOW require ice volumes in excess of the Last Glacial Maximum, when
345 ice sheets covered large parts of North America and Europe as well as Antarctica. Unlike at the
346 Last Glacial Maximum, it is thought that in the Cretaceous, ice was considerably more limited
347 and is, therefore, not sufficient to explain such high $\delta^{18}\text{O}_{\text{sw}}$ values. Any ice would also have to
348 be isotopically very light. Studies have also postulated that water could be stored as
349 (isotopically light) freshwater on land (e.g. Jacobs and Sahagian, 1993). As this study, however,
350 suggests that the latitudinal temperature gradient during the Early Cretaceous was less steep
351 than today, it is conceivable that the $\delta^{18}\text{O}_{\text{ice}}$ and any stored freshwater was also less extreme. If

352 the $\delta^{18}\text{O}_{\text{ice}}$ value was less negative, this would make it even harder to get $\delta^{18}\text{O}_{\text{sw}}$ values to 1‰
353 SMOW or more, as even greater ice volumes would be required. This is consistent with studies
354 of the Antarctic ice sheet during the early Miocene when the latitudinal temperature gradient
355 was less extreme and Antarctic temperatures were warmer than today resulting in significantly
356 higher $\delta^{18}\text{O}_{\text{ice}}$ values in the Miocene ice sheet (e.g. ca. -35‰ SMOW) than values today
357 (i.e. -45‰ to -55‰ SMOW) (Pekar and DeConto, 2006).

358 Alternatively, the high $\delta^{18}\text{O}_{\text{sw}}$ values could be caused by relatively high rates of
359 evaporation leading to higher salinities. Although, salinity can be estimated from salinity– $\delta^{18}\text{O}$
360 models for marine basins (e.g. Railsback et al., 1989), to reconcile our belemnite $\delta^{18}\text{O}$ data with
361 the Δ_{47} -derived temperatures, salinities in excess of 41 PSU are required (see also Wierzbowski
362 et al., 2018). As such, each of the sites examined here would need to be dominated by
363 evaporation. As the belemnite samples were derived from open marine systems (based upon
364 the presence of a fully marine fauna, including ammonites), high salinities contributing to high
365 $\delta^{18}\text{O}_{\text{sw}}$ values seems unlikely.

366 The marine carbonate $\delta^{18}\text{O}$ record also depends on seawater pH (Wallmann, 2004).
367 Seawater pH is strongly influenced by changes in $p\text{CO}_2$ (Zeebe, 1999, 2001; Wallmann, 2004).
368 An increase of seawater pH of 0.2–0.3 units, for example, is considered to result in a decrease
369 of about 0.22–0.33‰ in the $\delta^{18}\text{O}$ values of foraminiferal calcite, which would normally be
370 interpreted as a temperature increase of seawater, although the magnitude of the effect may
371 be species-dependent (Zeebe, 2001). During periods of high atmospheric CO_2 levels such as the
372 Cretaceous (Bernier and Kothavala, 2001; Wang et al., 2014; Witkowski et al., 2018), this pH
373 effect (Zeebe, 2001) if applicable to belemnites, would lead to an increase in the $\delta^{18}\text{O}$ value of
374 calcite. However, the magnitude of pH change in seawater needed to explain the observed
375 offset in $\delta^{18}\text{O}_{\text{sw}}$ value between an ice-free -1‰ SMOW and the average of our estimate of
376 +1.5‰ SMOW (using the Kim and O’Neil, 1997 equation) and scaling of ca. 0.1 pH unit for every

377 0.1‰ $\delta^{18}\text{O}$, means that oceans would need to be ca. 2.5 pH units more acidic. Such a
378 magnitude of change is not realistic (see Caldeira and Wickett, 2003).

379 Changes in the oxygen isotope composition of ancient oceans is a debated issue. Veizer
380 and Prokoph (2015) and Jaffrés et al. (2007) for example suggest that the $\delta^{18}\text{O}_{\text{sw}}$ value has
381 increased gradually through Earth's history, from -6‰ SMOW in the Cambrian to its present
382 value of ca. 0‰ SMOW. Other studies, applying the clumped isotope palaeothermometer,
383 indicate more or less constant $\delta^{18}\text{O}_{\text{sw}}$ values through geologic time (e.g. Ryb and Eiler, 2018;
384 Henkes, et al., 2018). Most models of the geological ^{18}O -cycle conclude that seawater/rock
385 interaction with silicates of oceanic crust at high and low temperatures balance each other and,
386 thus buffer the $\delta^{18}\text{O}_{\text{sw}}$ value at about $0(\pm 2)\%$ SMOW (Muehlenbachs and Clayton, 1976;
387 Holland, 1984). Hence, it has been considered that the $\delta^{18}\text{O}_{\text{sw}}$ value of the global ocean has not
388 changed significantly over time, but has been buffered by hydrothermal and weathering
389 processes (low-temperature interactions with silicates) at mid-ocean ridges and on ridge flanks,
390 based on results of ophiolite studies (e.g. Coogan et al., 2019). High-temperature alteration
391 (mainly via hydrothermal fluids) leads to an increase in $\delta^{18}\text{O}_{\text{sw}}$ values, while low-temperature
392 alteration (e.g. weathering processes) leave the ocean ^{18}O -depleted (Muehlenbachs and
393 Clayton, 1976; Holland, 1984; Muehlenbachs, 1998). These mass balance calculations, however,
394 do not rule out minor variations in the average $\delta^{18}\text{O}_{\text{sw}}$ value that could conceivably produce a
395 minor change towards more positive values reconciling our belemnite $\delta^{18}\text{O}$ data and
396 corresponding Δ_{47} -derived temperatures.

397 **5 Conclusions**

398 The Early Cretaceous Δ_{47} -derived temperatures of this study point to Arctic regions
399 above freezing. Our data argue against an extended ice sheet in the Northern Hemisphere and
400 shows congruence with TEX_{86} temperatures. Our clumped isotope-based temperature
401 reconstruction suggests the existence of a strongly reduced equator-to-pole temperature

402 gradient in the Northern Hemisphere. We find that modelling efforts are close to reproducing
403 the tropical temperatures when high atmospheric CO₂ levels are invoked, however, our data
404 suggests warmer temperatures at higher latitudes that are not shown in the models.

405 The results of this study indicate that it is unlikely that the oxygen isotope composition
406 of the seawater was homogenous. Our Early Cretaceous $\delta^{18}\text{O}_{\text{sw}}$ results are a conservative
407 reconstruction of a latitudinal gradient that shows a gentle decrease in values poleward and
408 also, using the Kim and O'Neil (1997) and Coplen (2007) equations plot in the upper portion or
409 wholly within the field of modern seawater. Early Cretaceous $\delta^{18}\text{O}_{\text{sw}}$ values with modern
410 characteristics implies some storage of light isotopes away from the ocean, e.g. as ice
411 accumulation on Antarctica. The constraints we provide on the oxygen isotope composition of
412 Early Cretaceous seawater, underpins our understanding of the evolution of the Earth's
413 temperature. Disregarding positive Early Cretaceous $\delta^{18}\text{O}_{\text{sw}}$ values results in an
414 underestimation of temperatures, most acute at middle and tropical latitudes.

415

416 **Acknowledgements**

417 Funding for this study was provided by a UK Natural Environment Research Council
418 (NERC) grant (NE/J020842/1) to GDP. We thank S. Hofmann, C. Schreiber (Goethe University
419 Frankfurt), N. Löffler, K. Methner and E. Krsnik (Senckenberg BIK-F) for their technical help.
420 Further supporting data can be accessed in Table 1 of Supporting information. The authors
421 declare no conflicts of interest. We would like to thank reviewers Sierra Petersen and Hubert
422 Wierzbowski for comprehensive and constructive reviews that greatly improved the
423 manuscript. Comments from Thomas Algeo also improved the manuscript. Further supporting
424 data can be accessed in the Supporting information and on Pangaea
425 (<https://doi.pangaea.de/10.1594/PANGAEA.907273>)

426

427 **References**

- 428 Aguado, R., Company, M., Tavera, J.M., 2000. The Berriasian/Valanginian boundary in the
429 Mediterranean region: New data from the Caravaca and Cehegín sections, SE Spain.
430 Cretac. Res. 21, 1-21. <https://doi.org/10.1006/cres.2000.0198>
- 431 Baraboshkin, E.Y., 2004. Boreal-Tethyan correlation of Lower Cretaceous ammonite scales.
432 Moscow Univ. Geol. Bull. 59, 9-20.
- 433 Barron, E.J., 1983. A warm, equable Cretaceous: The nature of the problem. Earth-Sci. Rev. 19,
434 305-338. [https://doi.org/10.1016/0012-8252\(83\)90001-6](https://doi.org/10.1016/0012-8252(83)90001-6)
- 435 Berner, R.A., Kothavala, Z., 2001. GEOCARB III: A revised model of atmospheric CO₂ over
436 phanerozoic time. Am. J. Sci. 301, 182-204. <https://doi.org/10.2475/ajs.301.2.182>
- 437 Bice, K.L., Huber, B.T., Norris, R.D., 2003. Extreme polar warmth during the Cretaceous
438 greenhouse? Paradox of the late Turonian $\delta^{18}\text{O}$ record at Deep Sea Drilling Project Site
439 511. Paleocyanography 18, 1031. <https://doi.org/10.1029/2002pa000848>
- 440 Brenner, D.C., Passey, B.H., Stolper, D.A., 2018. Influence of water on clumped-isotope bond
441 reordering kinetics in calcite. Geochim. Cosmochim. Acta 224, 42-63.
442 <https://doi.org/10.1016/j.gca.2017.12.026>
- 443 Caldeira, K., Wickett, M.E., 2003. Oceanography: Anthropogenic carbon and ocean pH. Nature
444 425, 365. <https://doi.org/10.1038/425365a>
- 445 Company, M., Tavera, J.M., 2015. Lower Valanginian ammonite biostratigraphy in the Subbetic
446 Domain (Betic Cordillera, southeastern Spain). Carnets Geol. 15, 71-88.
- 447 Coogan, L.A., Daëron, M., Gillis, K.M., 2019. Seafloor weathering and the oxygen isotope ratio in
448 seawater: Insight from whole-rock $\delta^{18}\text{O}$ and carbonate $\delta^{18}\text{O}$ and Δ_{47} from the Troodos
449 ophiolite. Earth Planet. Sci. Lett. 508, 41-50. <https://doi.org/10.1016/j.epsl.2018.12.014>

450 Coplen, T.B., 2007. Calibration of the calcite–water oxygen-isotope geothermometer at Devils
451 Hole, Nevada, a natural laboratory. *Geochim. Cosmochim. Acta* 71, 3948-3957.
452 <https://doi.org/10.1016/j.gca.2007.05.028>

453 Daëron, M., Blamart, D., Peral, M., Affek, H.P., 2016. Absolute isotopic abundance ratios and
454 the accuracy of Δ_{47} measurements. *Chem. Geol.* 442, 83-96.
455 <https://doi.org/10.1016/j.chemgeo.2016.08.014>

456 DeConto, R.M., Pollard, D., 2003. Rapid Cenozoic glaciation of Antarctica induced by declining
457 atmospheric CO₂. *Nature* 421, 245-249. <https://doi.org/10.1038/nature01290>

458 Dennis, K.J., Cochran, J.K., Landman, N.H., Schrag, D.P., 2013. The climate of the Late
459 Cretaceous: New insights from the application of the carbonate clumped isotope
460 thermometer to Western Interior Seaway macrofossil. *Earth Planet. Sci. Lett.* 362, 51-65.
461 <https://doi.org/10.1016/j.epsl.2012.11.036>

462 Ditchfield, P.W., 1997. High northern palaeolatitude Jurassic-Cretaceous palaeotemperature
463 variation: new data from Kong Karls Land, Svalbard. *Palaeogeogr. Palaeoclimatol.*
464 *Palaeoecol.* 130, 163-175. [https://doi.org/10.1016/S0031-0182\(96\)00054-5](https://doi.org/10.1016/S0031-0182(96)00054-5)

465 Dobretsov, N.L., Polyansky, O.P., Reverdatto, V.V., Babichev, A.V., 2013. Dynamics of the Arctic
466 and adjacent petroleum basins: a record of plume and rifting activity. *Russ. Geol.*
467 *Geophys.* 54, 888-902. <https://doi.org/10.1016/j.rgg.2013.07.009>

468 Donnadiou, Y., Puceat, E., Moiroud, M., Guillocheau, F., Deconinck, J.F., 2016. A better-
469 ventilated ocean triggered by Late Cretaceous changes in continental configuration. *Nat.*
470 *Commun.* 7, 10316. <https://doi.org/10.1038/ncomms10316>

471 Evans, D., Sahoo, N., Renema, W., Cotton, L.J., Müller, W., Todd, J.A., Saraswati, P.K., Stassen,
472 P., Ziegler, M., Pearson, P.N., Valdes, P.J., Affek, H.P., 2018. Eocene greenhouse climate
473 revealed by coupled clumped isotope-Mg/Ca thermometry. *Proc. Natl. Acad. Sci. U.S.A.*
474 115, 1174-1179. <https://doi.org/10.1073/pnas.1714744115>

475 Fiebig, J., Hofmann, S., Niklas, L., Lüdecke, T., Methner, K., Wacker, U., 2016. Slight pressure
476 imbalances can affect accuracy and precision of dual inlet-based clumped isotope
477 analysis. *Isotopes Environ. Health Stud.* 52, 12-28.
478 <https://doi.org/10.1080/10256016.2015.1010531>

479 Frakes, L.A., 1979. *Climates throughout geologic time*. Elsevier, Amsterdam.

480 Frakes, L.A., Francis, J.E., 1988. A guide to Phanerozoic cold polar climates from high-latitude
481 ice-rafting in the Cretaceous. *Nature* 333, 547-549. <https://doi.org/10.1038/333547a0>

482 Ghosh, P., Adkins, J., Affek, H., Balta, B., Guo, W., Schauble, E.A., Schrag, D., Eiler, J.M., 2006.
483 ^{13}C – ^{18}O bonds in carbonate minerals: A new kind of paleothermometer. *Geochim.*
484 *Cosmochim. Acta* 70, 1439-1456. <https://doi.org/10.1016/j.gca.2005.11.014>

485 Gradstein, F.M., Ogg, J.G., Schmitz, M.D., Ogg, G.M., 2012. *The Geologic Time Scale 2012*.
486 Elsevier, p. 1176.

487 Grasby, S.E., McCune, G.E., Beauchamp, B., Galloway, J.M., 2017. Lower Cretaceous cold snaps
488 led to widespread glendonite occurrences in the Sverdrup Basin, Canadian High Arctic.
489 *Geol. Soc. Am. Bull.* 129, 771-787. <https://doi.org/10.1130/B31600.1>

490 Hemingway, J.E., Riddler, G.P., 1982. Basin inversion in North Yorkshire. *T. I. Min. Metall. B* 91,
491 B175-B186.

492 Henkes, G.A., Passey, B.H., Wanamaker, A.D., Grossman, E.L., Ambrose, W.G., Carroll, M.L.,
493 2013. Carbonate clumped isotope compositions of modern marine mollusk and
494 brachiopod shells. *Geochim. Cosmochim. Acta* 106, 307-325.
495 <https://doi.org/10.1016/j.gca.2012.12.020>

496 Henkes, G.A., Passey, B.H., Grossman, E.L., Shenton, B.J., Yancey, T.E., Pérez-Huerta, A., 2018.
497 Temperature evolution and the oxygen isotope composition of Phanerozoic oceans from
498 carbonate clumped isotope thermometry. *Earth Planet. Sci. Lett.* 490, 40-50.
499 <https://doi.org/10.1016/j.epsl.2018.02.001>

500 Holland, H.D., 2004. The geologic history of seawater, in: Elderfield, H., Holland, H.D., Turekian,
501 K.K. (Eds.), *Treatise on Geochemistry*, Vol. 6. The Oceans and Marine Geochemistry.
502 Elsevier Pergamon, Kidlington, Oxford, pp. 583–625.

503 Holliday, D.W., 1999. Palaeotemperatures, thermal modelling and depth of burial studies in
504 northern and eastern England. *Proc. Yorkshire Geol. Soc.* 52, 337-352.
505 <https://doi.org/10.1144/pygs.52.4.337>

506 Huber, B.T., Hodell, D.A., Hamilton, C.P., 1995. Middle-Late Cretaceous climate of the southern
507 high latitudes: Stable isotopic evidence for minimal equator-to-pole thermal gradients.
508 *Geol. Soc. Am. Bull.* 107, 1164-1191. [https://doi.org/10.1130/0016-](https://doi.org/10.1130/0016-7606(1995)107<1164:MLCCOT>2.3.CO;2)
509 [7606\(1995\)107<1164:MLCCOT>2.3.CO;2](https://doi.org/10.1130/0016-7606(1995)107<1164:MLCCOT>2.3.CO;2)

510 Huber, B.T., MacLeod, K.G., Watkins, D.K., Coffin, M.F., 2018. The rise and fall of the Cretaceous
511 hot greenhouse climate. *Glob. Planet. Change* 167, 1-23.
512 <https://doi.org/10.1016/j.gloplacha.2018.04.004>

513 Hurum, J.H., Milan, J., Hammer, O., Midtkandal, I., Amundsen, H., Saether, B., 2006. Tracking
514 polar dinosaurs - new finds from the Lower Cretaceous of Svalbard. *Norw. J. Geol.* 86,
515 397-402.

516 Jacobs, D.K., Sahagian, D.L., 1993. Climate-induced fluctuations in sea level during non-glacial
517 times. *Nature* 361, 710-712. <https://doi.org/10.1038/361710a0>

518 Jaffrés, J.B.D., Shields, G.A., Wallmann, K., 2007. The oxygen isotope evolution of seawater: A
519 critical review of a long-standing controversy and an improved geological water cycle
520 model for the past 3.4 billion years. *Earth-Sci. Rev.* 83, 83-122.
521 <https://doi.org/10.1016/j.earscirev.2007.04.002>

522 Janssen, N.M.M., 2003. Mediterranean Neocomian belemnites, part 2: The Berriasian-
523 Valanginian boundary in southeast Spain (Río Argos, Cañada Lengua and Tornajo). *Scr.*
524 *Geol.* 126, 121-183.

525 Jenkyns, H.C., Forster, A., Schouten, S., Sinninghe Damsté, J.S., 2004. High temperatures in the
526 late Cretaceous Arctic Ocean. *Nature* 432, 888-892. <https://doi.org/10.1038/nature03143>

527 Jenkyns, H.C., Schouten-Huibers, L., Schouten, S., Sinninghe Damsté, J.S., 2012. Warm Middle
528 Jurassic–Early Cretaceous high-latitude sea-surface temperatures from the Southern
529 Ocean. *Clim. Past* 8, 215-226. <https://doi.org/10.5194/cp-8-215-2012>

530 Kelson, J.R., Huntington, K.W., Schauer, A.J., Saenger, C., Lechler, A.R., 2017. Toward a universal
531 carbonate clumped isotope calibration: Diverse synthesis and preparatory methods
532 suggest a single temperature relationship. *Geochim. Cosmochim. Acta* 197, 104-131.
533 <https://doi.org/10.1016/j.gca.2016.10.010>

534 Kim, S.-T., O'Neil, J.R., 1997. Equilibrium and nonequilibrium oxygen isotope effects in synthetic
535 carbonates. *Geochim. Cosmochim. Acta* 61, 3461-3475. [https://doi.org/10.1016/S0016-](https://doi.org/10.1016/S0016-7037(97)00169-5)
536 [7037\(97\)00169-5](https://doi.org/10.1016/S0016-7037(97)00169-5)

537 Kim, S.-T., Mucci, A., Taylor, B.E., 2007. Phosphoric acid fractionation factors for calcite and
538 aragonite between 25 and 75 °C: Revisited. *Chem. Geol.* 246, 135-146.
539 <https://doi.org/10.1016/j.chemgeo.2007.08.005>

540 Kim, J.-H., van der Meer, J., Schouten, S., Helmke, P., Willmott, V., Sangiorgi, F., Koç, N.,
541 Hopmans, E.C., Damsté, J.S.S., 2010. New indices and calibrations derived from the
542 distribution of crenarchaeal isoprenoid tetraether lipids: Implications for past sea surface
543 temperature reconstructions. *Geochim. Cosmochim. Acta* 74, 4639-4654.
544 <https://doi.org/10.1016/j.gca.2010.05.027>

545 Klett, T.R., Wandrey, C.J., Pitman, J.K., 2011. Geology and petroleum potential of the north and
546 east margins of the Siberian Craton, north of the Arctic Circle. *Arct. Pet. Geol.* 35, 413-
547 431. <https://doi.org/10.1144/M35.27>

548 Klug, C., Schweigert, G., Fuchs, D., Kruta, I., Tischlinger, H., 2016. Adaptations to squid-style
549 high-speed swimming in Jurassic belemnitids. *Biol. Lett.* 12, 1-5.
550 <https://doi.org/10.1098/rsbl.2015.0877>

551 Kump, L.R., Pollard, D., 2008. Amplification of Cretaceous warmth by biological cloud
552 feedbacks. *Science* 320, 195. <https://doi.org/10.1126/science.1153883>

553 LeGrande, A.N., Schmidt, G.A., 2006. Global gridded data set of the oxygen isotopic
554 composition in seawater. *Geophys. Res. Lett.* 33, 1-5.
555 <https://doi.org/10.1029/2006gl026011>

556 Lindquist, S.J., 1999. The Timan-Pechora Basin province of northwest Arctic Russia; Domanik,
557 Paleozoic total petroleum system. USGS Open-File Report 99-50, 1-24.
558 <https://doi.org/10.3133/ofr9950G>

559 Littler, K., Robinson, S.A., Bown, P.R., Nederbragt, A.J., Pancost, R.D., 2011. High sea-surface
560 temperatures during the Early Cretaceous Epoch. *Nat. Geosci.* 4, 169-172.
561 <https://doi.org/10.1038/ngeo1081>

562 Locarnini, R.A., Mishonov, A.V., Antonov, J.I., Boyer, T.P., Garcia, H.E., Baranova, O.K., Zweng,
563 M.M., Paver, C.R., Reagan, J.R., Johnson, D.R., Hamilton, M., Seidov, D., 2013. World
564 Ocean Atlas 2013, Volume 1: Temperature.

565 Lunt, D.J., Farnsworth, A., Loptson, C., Foster, G.L., Markwick, P., Brien, C.L., Pancost, R.D.,
566 Robinson, S.A., Wrobel, N., 2016. Palaeogeographic controls on climate and proxy
567 interpretation. *Clim. Past* 12, 1181-1198. <https://doi.org/10.5194/cp-12-1181-2016>

568 Marshall, J.D., 1992. Climatic and oceanographic isotopic signals from the carbonate rock
569 record and their preservation. *Geol. Mag.* 129, 143-160.
570 <https://doi.org/10.1017/s0016756800008244>

571 McArthur, J.M., Mutterlose, J., Price, G.D., Rawson, P.F., Ruffell, A., Thirlwall, M.F., 2004.
572 Belemnites of Valanginian, Hauterivian and Barremian age: Sr-isotope stratigraphy,

573 composition ($^{87}\text{Sr}/^{86}\text{Sr}$, $\delta^{13}\text{C}$, $\delta^{18}\text{O}$, Na, Sr, Mg), and palaeo-oceanography. *Palaeogeogr.*
574 *Palaeoclimatol. Palaeoecol.* 202, 253-272. [https://doi.org/10.1016/s0031-0182\(03\)00638-](https://doi.org/10.1016/s0031-0182(03)00638-2)
575 2

576 McArthur, J.M., Janssen, N.M.M., Reboulet, S., Leng, M.J., Thirlwall, M.F., van de Schootbrugge,
577 B., 2007. Palaeotemperatures, polar ice-volume, and isotope stratigraphy (Mg/Ca, $\delta^{18}\text{O}$,
578 $\delta^{13}\text{C}$, $^{87}\text{Sr}/^{86}\text{Sr}$): The Early Cretaceous (Berriasian, Valanginian, Hauterivian). *Palaeogeogr.*
579 *Palaeoclimatol. Palaeoecol.* 248, 391-430. <https://doi.org/10.1016/j.palaeo.2006.12.015>

580 McConnaughey, T., 1989. ^{13}C and ^{18}O isotopic disequilibrium in biological carbonates: II. *In vitro*
581 simulation of kinetic isotope effects. *Geochim. Cosmochim. Acta* 53, 163-171.
582 [https://doi.org/10.1016/0016-7037\(89\)90283-4](https://doi.org/10.1016/0016-7037(89)90283-4)

583 Meyer, K.W., Petersen, S.V., Lohmann, K.C., Winkelstern, I.Z., 2018. Climate of the Late
584 Cretaceous North American Gulf and Atlantic Coasts. *Cretac. Res.* 89, 160-173.
585 <https://doi.org/10.1016/j.cretres.2018.03.017>

586 Miller, K.G., 2009. Broken greenhouse windows. *Nat. Geosci.* 2, 465-466.
587 <https://doi.org/10.1038/ngeo563>

588 Muehlenbachs, K., Clayton, R.N., 1976. Oxygen isotope composition of the oceanic crust and its
589 bearing on seawater. *J. Geophys. Res.* 81, 4365-4369.
590 <https://doi.org/10.1029/JB081i023p04365>

591 Muehlenbachs, K., 1998. The oxygen isotopic composition of the oceans, sediments and the
592 seafloor. *Chem. Geol.* 145, 263-273. [https://doi.org/10.1016/S0009-2541\(97\)00147-2](https://doi.org/10.1016/S0009-2541(97)00147-2)

593 Mutterlose, J., Malkoc, M., Schouten, S., Sinninghe Damsté, J.S., Forster, A., 2010. TEX_{86} and
594 stable $\delta^{18}\text{O}$ paleothermometry of early Cretaceous sediments: Implications for belemnite
595 ecology and paleotemperature proxy application. *Earth Planet. Sci. Lett.* 298, 286–298.
596 <https://doi.org/10.1016/j.epsl.2010.07.043>

597 Mutterlose, J., Malkoc, M., Schouten, S., Sinninghe Damsté, J.S., 2012. Reconstruction of
598 vertical temperature gradients in past oceans — Proxy data from the Hauterivian–early
599 Barremian (Early Cretaceous) of the Boreal Realm. *Palaeogeogr. Palaeoclimatol.*
600 *Palaeoecol.* 363-364, 135-143. <https://doi.org/10.1016/j.palaeo.2012.09.006>

601 Naafs, B.D.A., Pancost, R.D., 2016. Sea-surface temperature evolution across Aptian Oceanic
602 Anoxic Event 1a. *Geology* 44, 959-962. <https://doi.org/10.1130/g38575.1>

603 Nunn, E.V., Price, G.D., Gröcke, D.R., Baraboshkin, E.Y., Leng, M.J., Hart, M.B., 2010. The
604 Valanginian positive carbon isotope event in Arctic Russia: Evidence from terrestrial and
605 marine isotope records and implications for global carbon cycling. *Cretac. Res.* 31, 577-
606 592. <https://doi.org/10.1016/j.cretres.2010.07.007>

607 O'Brien, C.L., Robinson, S.A., Pancost, R.D., Sinninghe Damsté, J.S., Schouten, S., Lunt, D.J.,
608 Alsenz, H., Bornemann, A., Bottini, C., Brassell, S.C., Farnsworth, A., Forster, A., Huber,
609 B.T., Inglis, G.N., Jenkyns, H.C., Linnert, C., Littler, K., Markwick, P., McAnena, A.,
610 Mutterlose, J., Naafs, B.D.A., Püttmann, W., Sluijs, A., van Helmond, N.A.G.M., Vellekoop,
611 J., Wagner, T., Wrobel, N.E., 2017. Cretaceous sea-surface temperature evolution:
612 Constraints from TEX₈₆ and planktonic foraminiferal oxygen isotopes. *Earth-Sci. Rev.* 172,
613 224-247. <https://doi.org/10.1016/j.earscirev.2017.07.012>

614 O'Connor, L.K., Robinson, S.A., Naafs, B.D.A., Jenkyns, H.C., Henson, S., Clarke, M., Pancost,
615 R.D., 2019. Late Cretaceous temperature evolution of the southern high latitudes: a TEX₈₆
616 perspective. *Paleoceanography and Paleoclimatology* 34, 436-454.
617 <https://doi.org/10.1029/2018pa003546>

618 Passey, B.H., Henkes, G.A., 2012. Carbonate clumped isotope bond reordering and
619 geospeedometry. *Earth Planet. Sci. Lett.* 351-352, 223-236.
620 <https://doi.org/10.1016/j.epsl.2012.07.021>

621 Pekar, S.F., DeConto, R.M., 2006. High-resolution ice-volume estimates for the early Miocene:
622 Evidence for a dynamic ice sheet in Antarctica. *Palaeogeogr. Palaeoclimatol. Palaeoecol.*
623 231, 101-109. <https://doi.org/10.1016/j.palaeo.2005.07.027>

624 Petersen, S.V., Schrag, D.P., 2015. Antarctic ice growth before and after the Eocene-Oligocene
625 transition: New estimates from clumped isotope paleothermometry. *Paleoceanography*
626 30, 1305-1317. <https://doi.org/10.1002/2014PA002769>

627 Petersen, S.V., Tabor, C.R., Lohmann, K.C., Poulsen, C.J., Meyer, K.W., Carpenter, S.J., Erickson,
628 J.M., Matsunaga, K.K.S., Smith, S.Y., Sheldon, N.D., 2016. Temperature and salinity of the
629 Late Cretaceous Western Interior Seaway. *Geology* 44, 903-906.
630 <https://doi.org/10.1130/g38311.1>

631 Petersen, S.V., Defliese, W.F., Saenger, C., Daëron, M., Huntington, K.W., John, C.M., Kelson,
632 J.R., Coleman, A.S., Kluge, T., Olack, G.A., Schauer, A.J., Bajnai, D., Bonifacie, M.,
633 Breitenbach, S.F., Fiebig, J., Fernandez, A.B., Henkes, G.A., Hodell, D., Katz, A., Kele, S.,
634 Lohmann, K.C., Passey, B.H., Peral, M.Y., Petrizzo, D.A., Rosenheim, B.E., Tripathi, A.,
635 Venturelli, R., Young, E.D., Winkelstern, I.Z., 2019. Effects of improved ¹⁷O correction on
636 interlaboratory agreement in clumped isotope calibrations, estimates of mineral-specific
637 offsets, and temperature dependence of acid digestion fractionation. *Geochem. Geophys.*
638 *Geosyst.* 20, 3495-3519. <https://doi.org/10.1029/2018GC008127>

639 Poulsen, C.J., Pollard, D., White, T.S., 2007. General circulation model simulation of the $\delta^{18}\text{O}$
640 content of continental precipitation in the middle Cretaceous: A model-proxy
641 comparison. *Geology* 35, 199-202. <https://doi.org/10.1130/G23343A.1>

642 Price, G.D., 1999. The evidence and implications of polar ice during the Mesozoic. *Earth-Sci.*
643 *Rev.* 48, 183-210. [https://doi.org/10.1016/s0012-8252\(99\)00048-3](https://doi.org/10.1016/s0012-8252(99)00048-3)

644 Price, G.D., Ruffell, A.H., Jones, C.E., Kalin, R.M., Mutterlose, J., 2000. Isotopic evidence for
645 temperature variation during the early Cretaceous (late Ryazanian-mid-Hauterivian). *J.*
646 *Geol. Soc.* 157, 335-343. <https://doi.org/10.1144/jgs.157.2.335>

647 Price, G.D., Nunn, E.V., 2010. Valanginian isotope variation in glendonites and belemnites from
648 Arctic Svalbard: Transient glacial temperatures during the Cretaceous greenhouse.
649 *Geology* 38, 251-254. <https://doi.org/10.1130/g30593.1>

650 Price, G.D., Passey, B.H., 2013. Dynamic polar climates in a greenhouse world: Evidence from
651 clumped isotope thermometry of Early Cretaceous belemnites. *Geology* 41, 923-926.
652 <https://doi.org/10.1130/g34484.1>

653 Price, G.D., Hart, M.B., Wilby, P.R., Page, K.N., 2015. Isotopic analysis of Jurassic (Calloviaian)
654 mollusks from the Christian Malford lagerstätte (UK): Implications for ocean water
655 temperature estimates based on belemnoids. *Palaios* 30, 645-654.
656 <https://doi.org/10.2110/palo.2014.106>

657 Price, G.D., Janssen, N.M.M., Martinez, M., Company, M., Vandeveld, J.H., Grimes, S.T., 2018.
658 A high-resolution belemnite geochemical analysis of Early Cretaceous (Valanginian-
659 Hauterivian) environmental and climatic perturbations. *Geochem. Geophys. Geosyst.* 19,
660 3832-3843. <https://doi.org/10.1029/2018gc007676>

661 Pucéat, E., Lecuyer, C., Sheppard, S.M.F., Dromart, G., Reboulet, S., Grandjean, P., 2003.
662 Thermal evolution of Cretaceous Tethyan marine waters inferred from oxygen isotope
663 composition of fish tooth enamels. *Paleoceanography* 18, 1029.
664 <https://doi.org/10.1029/2002pa000823>

665 Railsback, L.B., Anderson, T.F., Ackerly, S.C., Cisne, J.L., 1989. Paleoceanographic modeling of
666 temperature-salinity profiles from stable isotopic data. *Paleoceanography* 4, 585-591.
667 <https://doi.org/10.1029/PA004i005p00585>

668 Rawson, P.F., 1973. Lower Cretaceous (Ryazanian-Barremian) marine connections and
669 cephalopod migrations between the Tethyan and Boreal Realms, in: Casey, R., Rawson,
670 P.F. (Eds.), *The Boreal Lower Cretaceous*. Seel House Press, Liverpool, pp. 131-144.

671 Reboulet, S., Szives, O., Aguirre-Urreta, B., Barragán, R., Company, M., Frau, C., Kakabadze,
672 M.V., Klein, J., Moreno-Bedmar, J.A., Lukeneder, A., Pictet, A., Ploch, I., Raisossadat, S.N.,
673 Vašíček, Z., Baraboshkin, E.J., Mitta, V.V., 2018. Report on the 6th International Meeting
674 of the IUGS Lower Cretaceous Ammonite Working Group, the Kilian Group (Vienna,
675 Austria, 20th August 2017). *Cretac. Res.* 91, 100-110.
676 <https://doi.org/10.1016/j.cretres.2018.05.008>

677 Reicherter, K., Wiedmann, J., Herbin, J.P., 1996. Distribution of organic-rich sediments in
678 Subbetic sections during the Aptian-Turonian (Betic Cordillera, Southern Spain). *Rev. Soc.*
679 *Geol. Esp.* 9, 75-88.

680 Rogov, M.A., Ershova, V.B., Shchepetova, E.V., Zakharov, V.A., Pokrovsky, B.G., Khudoley, A.K.,
681 2017. Earliest Cretaceous (late Berriasian) glendonites from Northeast Siberia revise the
682 timing of initiation of transient Early Cretaceous cooling in the high latitudes. *Cretac. Res.*
683 71, 102-112. <https://doi.org/10.1016/j.cretres.2016.11.011>

684 Ryb, U., Eiler, J.M., 2018. Oxygen isotope composition of the Phanerozoic ocean and a possible
685 solution to the dolomite problem. *Proc. Natl. Acad. Sci. U.S.A.* 115, 6602-6607.
686 <https://doi.org/10.1073/pnas.1719681115>

687 Sælen, G., 1989. Diagenesis and construction of the belemnite rostrum. *Palaeontology* 32, 765-
688 797.

689 Sagoo, N., Valdes, P., Flecker, R., Gregoire, L.J., 2013. The Early Eocene equable climate
690 problem: Can perturbations of climate model parameters identify possible solutions?
691 *Philos. T. R. Soc. A* 371, 20130123. <https://doi.org/10.1098/rsta.2013.0123>

692 Schmidt, G.A., Mysak, L.A., 1996. Can increased poleward oceanic heat flux explain the warm
693 Cretaceous climate? *Paleoceanography* 11, 579-593. <https://doi.org/10.1029/96pa01851>

694 van de Schootbrugge, B., Föllmi, K.B., Bulot, L.G., Burns, S.J., 2000. Paleoceanographic changes
695 during the early Cretaceous (Valanginian-Hauterivian): evidence from oxygen and carbon
696 stable isotopes. *Earth Planet. Sci. Lett.* 181, 15-31. [https://doi.org/10.1016/S0012-
697 821X\(00\)00194-1](https://doi.org/10.1016/S0012-821X(00)00194-1)

698 Scotese, C.R., 2014. Atlas of Early Cretaceous Paleogeographic Maps, PALEOMAP Atlas for
699 ArcGIS, volume 2, The Cretaceous, Maps 23-31, Mollweide Projection, Evanston, IL, USA.

700 Shackleton, N.J., Kennett, J.P., 1975. Paleotemperature history of the Cenozoic and the
701 initiation of antarctic glaciation: oxygen and carbon isotope analyses in DSDP sites 277,
702 279, and 281. *Deep Sea Drilling Project Initial Reports* 29, 743-755.
703 <https://doi.org/10.2973/dsdp.proc.29.117.1975>

704 Shulgina, N.I., Burdykina, M.D., Basov, V.A., Arhus, N., 1994. Distribution of ammonites,
705 foraminifera and dinoflagellate cysts in the Lower Cretaceous reference sections of the
706 Khatanga Basin, and Boreal Valanginian biogeography. *Cretac. Res.* 15, 1-16.
707 <https://doi.org/10.1006/cres.1994.1001>

708 Słowakiewicz, M., Tucker, M.E., Vane, C.H., Harding, R., Collins, A., Pancost, R.D., 2015. Shale-
709 gas potential of the mid-Carboniferous Bowland-Hodder Unit in the Cleveland Basin
710 (Yorkshire), central Britain. *J. Pet. Geol.* 38, 59-75. <https://doi.org/10.1111/jpg.12598>

711 Spicer, R.A., Ahlberg, A., Herman, A.B., Hofmann, C.-C., Raikevich, M., Valdes, P.J., Markwick,
712 P.J., 2008. The Late Cretaceous continental interior of Siberia: A challenge for climate
713 models. *Earth Planet. Sci. Lett.* 267, 228-235. <https://doi.org/10.1016/j.epsl.2007.11.049>

714 Spicer, R.A., Herman, A.B., 2010. The Late Cretaceous environment of the Arctic: A quantitative
715 reassessment based on plant fossils. *Palaeogeogr. Palaeoclimatol. Palaeoecol.* 295, 423-
716 442. <https://doi.org/10.1016/j.palaeo.2010.02.025>

717 Stevens, K., Mutterlose, J., Schweigert, G., 2014. Belemnite ecology and the environment of the
718 Nusplingen Plattenkalk (Late Jurassic, southern Germany): Evidence from stable isotope
719 data. *Lethaia* 47, 512-523. <https://doi.org/10.1111/let.12076>

720 Super, J.R., Chin, K., Pagani, M., Li, H., Tabor, C., Harwood, D.M., Hull, P.M., 2018. Late
721 Cretaceous climate in the Canadian Arctic: Multi-proxy constraints from Devon Island.
722 *Palaeogeogr. Palaeoclimatol. Palaeoecol.* 504, 1-22.
723 <https://doi.org/10.1016/j.palaeo.2018.03.004>

724 Tarduno, J.A., Brinkman, D.B., Renne, P.R., Cottrell, R.D., Scher, H., Castillo, P., 1998. Evidence
725 for extreme climatic warmth from Late Cretaceous Arctic vertebrates. *Science* 282, 2241-
726 2244. <https://doi.org/10.1126/science.282.5397.2241>

727 Tierney, J.E., Tingley, M.P., 2014. A Bayesian, spatially-varying calibration model for the TEX₈₆
728 proxy. *Geochim. Cosmochim. Acta* 127, 83-106.
729 <https://doi.org/10.1016/j.gca.2013.11.026>

730 Upchurch, G.R., Kiehl, J., Shields, C., Scherer, J., Scotese, C., 2015. Latitudinal temperature
731 gradients and high-latitude temperatures during the latest Cretaceous: Congruence of
732 geologic data and climate models. *Geology* 43, 683-686.
733 <https://doi.org/10.1130/g36802.1>

734 Veizer, J., 1974. Chemical diagenesis belemnite shells possible consequences for
735 paleotemperature determinations. *Neues Jahrb. Geol. Palaontol. Abhand.* 147, 91-111.

736 Veizer, J., Prokoph, A., 2015. Temperatures and oxygen isotopic composition of Phanerozoic
737 oceans. *Earth-Sci. Rev.* 146, 92-104. <https://doi.org/10.1016/j.earscirev.2015.03.008>

738 Vickers, M.L., Price, G.D., Jerrett, R.M., Watkinson, M., 2016. Stratigraphic and geochemical
739 expression of Barremian–Aptian global climate change in Arctic Svalbard. *Geosphere* 12,
740 1594-1605. <https://doi.org/10.1130/ges01344.1>

741 Vickers, M.L., Bajnai, D., Price, G.D., Linckens, J., Fiebig, J., 2019. Southern high latitude warmth
742 during Jurassic–Cretaceous: New evidence from clumped isotope thermometry. *Geology*
743 47, 724-728. <https://doi.org/10.1130/G46263.1>

744 Voigt, S., Wilmsen, M., Mortimore, R.N., Voigt, T., 2003. Cenomanian palaeotemperatures
745 derived from the oxygen isotopic composition of brachiopods and belemnites: evaluation
746 of Cretaceous palaeotemperature proxies. *Int. J. Earth Sci.* 92, 285-299.
747 <https://doi.org/10.1007/s00531-003-0315-1>

748 Wacker, U., Fiebig, J., Tödter, J., Schöne, B.R., Bahr, A., Friedrich, O., Tütken, T., Gischler, E.,
749 Joachimski, M.M., 2014. Empirical calibration of the clumped isotope paleothermometer
750 using calcites of various origins. *Geochim. Cosmochim. Acta* 141, 127-144.
751 <https://doi.org/10.1016/j.gca.2014.06.004>

752 Wallmann, K., 2004. Impact of atmospheric CO₂ and galactic cosmic radiation on Phanerozoic
753 climate change and the marine δ¹⁸O record. *Geochem. Geophys. Geosyst.* 5, 1-29.
754 <https://doi.org/10.1029/2003gc000683>

755 Wang, Y., Huang, C., Sun, B., Quan, C., Wu, J., Lin, Z., 2014. Paleo-CO₂ variation trends and the
756 Cretaceous greenhouse climate. *Earth-Sci. Rev.* 129, 136-147.
757 <https://doi.org/10.1016/j.earscirev.2013.11.001>

758 White, T., Gonzalez, L., Ludvigson, G., Poulsen, C., 2001. Middle Cretaceous greenhouse
759 hydrologic cycle of North America. *Geology* 29, 363-366. [https://doi.org/10.1130/0091-
760 7613\(2001\)029<0363:Mcghco>2.0.Co;2](https://doi.org/10.1130/0091-7613(2001)029<0363:Mcghco>2.0.Co;2)

761 Wierzbowski, H., Rogov, M.A., Matyja, B.A., Kiselev, D., Ippolitov, A., 2013. Middle–Upper
762 Jurassic (Upper Callovian–Lower Kimmeridgian) stable isotope and elemental records of
763 the Russian Platform: Indices of oceanographic and climatic changes. *Glob. Planet.*
764 *Change* 107, 196-212. <https://doi.org/10.1016/j.gloplacha.2013.05.011>

765 Wierzbowski, H., Bajnai, D., Wacker, U., Rogov, M.A., Fiebig, J., Tesakova, E.M., 2018. Clumped
766 isotope record of salinity variations in the Subboreal Province at the middle–late Jurassic
767 transition. *Glob. Planet. Change* 167, 172-189.
768 <https://doi.org/10.1016/j.gloplacha.2018.05.014>

769 Witkowski, C.R., Weijers, J.W.H., Blais, B., Schouten, S., Sinninghe Damsté, J.S., 2018. Molecular
770 fossils from phytoplankton reveal secular $p\text{CO}_2$ trend over the Phanerozoic. *Sci. Adv.* 4,
771 eaat4556. <https://doi.org/10.1126/sciadv.aat4556>

772 Young, A., Flament, N., Maloney, K., Williams, S., Matthews, K., Zahirovic, S., Müller, R.D., 2019.
773 Global kinematics of tectonic plates and subduction zones since the late Paleozoic Era.
774 *Geosci. Front.* 10, 989-1013. <https://doi.org/10.1016/j.gsf.2018.05.011>

775 Zakharov, V.A., Bogomolov, Y.I., Il'ina, V.I., Konstantinov, A.G., Kurushin, N.I., Lebedeva, N.K.,
776 Meledina, S.V., Nikitenko, B.L., Sobolev, E.S., Shurygin, B.N., 1997. Boreal zonal standard
777 and biostratigraphy of the Siberian Mesozoic. *Russ. Geol. Geophys.* 38, 965-993.

778 Zeebe, R.E., 1999. An explanation of the effect of seawater carbonate concentration on
779 foraminiferal oxygen isotopes. *Geochim. Cosmochim. Acta* 63, 2001-2007.
780 [https://doi.org/10.1016/S0016-7037\(99\)00091-5](https://doi.org/10.1016/S0016-7037(99)00091-5)

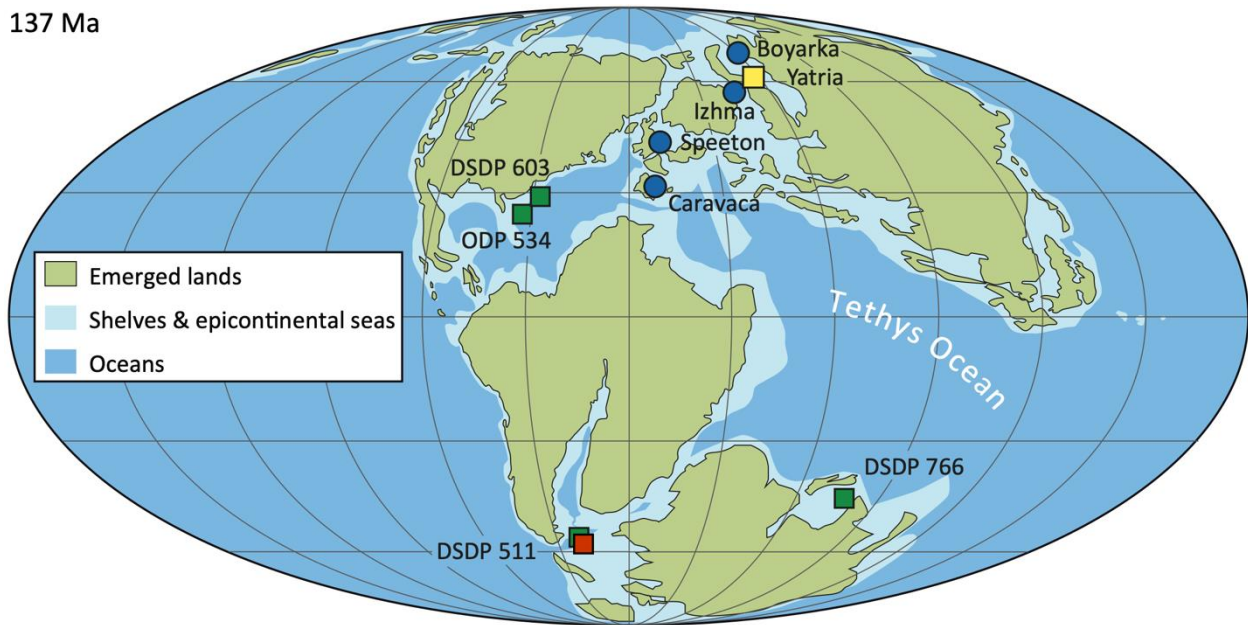
781 Zeebe, R.E., 2001. Seawater pH and isotopic paleotemperatures of Cretaceous ocean.
782 *Palaeogeogr. Palaeoclimatol. Palaeoecol.* 170, 49-57. [https://doi.org/10.1016/S0031-](https://doi.org/10.1016/S0031-0182(01)00226-7)
783 [0182\(01\)00226-7](https://doi.org/10.1016/S0031-0182(01)00226-7)

784 Zhou, J., Poulsen, C.J., Pollard, D., White, T.S., 2008. Simulation of modern and middle
785 Cretaceous marine $\delta^{18}\text{O}$ with an ocean-atmosphere general circulation model.
786 *Paleoceanography* 23, PA3223. <https://doi.org/10.1029/2008pa001596>

787 Zhu, J., Poulsen, C.J., Tierney, J.E., 2019. Simulation of Eocene extreme warmth and high climate
788 sensitivity through cloud feedbacks. *Sci. Adv.* 5, eaax1874.
789 <https://doi.org/10.1126/sciadv.aax1874>

791 **Figures**

137 Ma

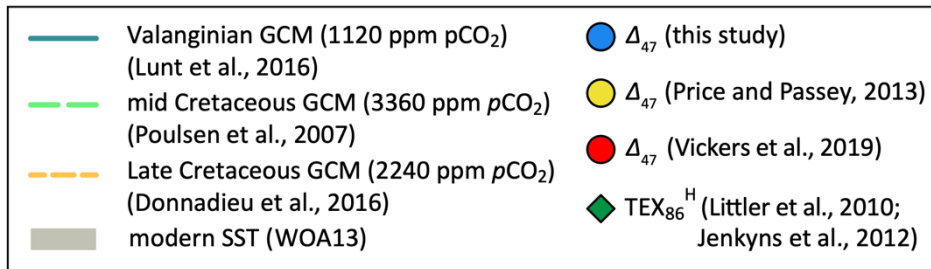
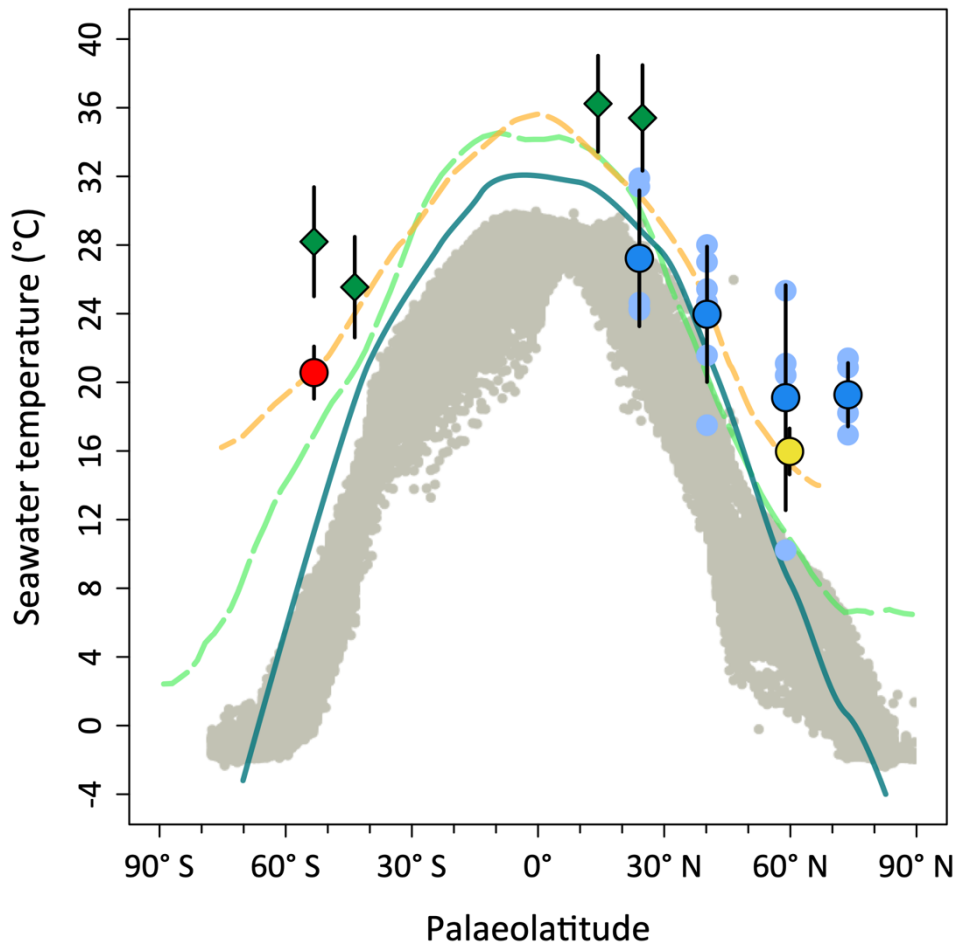


792
793 **Fig. 1.** Early Cretaceous palaeogeographic reconstruction with locations of the discussed study
794 sites. Map modified after Scotese (2014). Blue circles = data from this study; green squares =
795 location of published Early Cretaceous TEX₈₆ data (Littler et al. 2011; Jenkyns et al. 2012). The
796 locations of additional published Δ_{47} -based temperature data are marked with a yellow square
797 (Price and Passey, 2013) and a red square (Vickers et al. 2019). The palaeolatitude estimates are
798 consistent with Young et al. (2019) that are used for Figs 3 and 4.

		Tethyan ammonite zonation	Sub-Boreal ammonite zonation	Boreal (Siberian) ammonite zonation		
Valanginian	Upper	Criosarasinella furcillata	Endemoceras amblygonium	Homolsomites bojarkensis		
			Eleniceras paucinodum	Dichotomites bidichotomus	Neocraspedites kotschetkovi	
			Stolcoceras tuberculatum		Dichotomites bidichotomus	
		Neocomites peregrinus	Dichotomites		Polyptychites triplodiptychus	
			Prodichotomites		Polyptychites polyptychus	
	Lower	Karakaschiceras inostranzewi		Polyptychites	Polyptychites michalskii	
		Neocomites neocomiensiformis	Astieriptychites astieriptychus			
		Tirnovella pertransiens	Platylenticeras	Polyptychites quadrifidus	Neotollia klimovskiensis	
	Berriasian	Upper	Tirnovella apillensis	Peregrinoceras albidum	Tollia tolli	
				Surites stenomphalus		

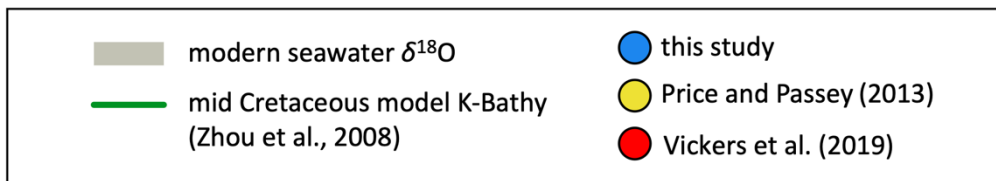
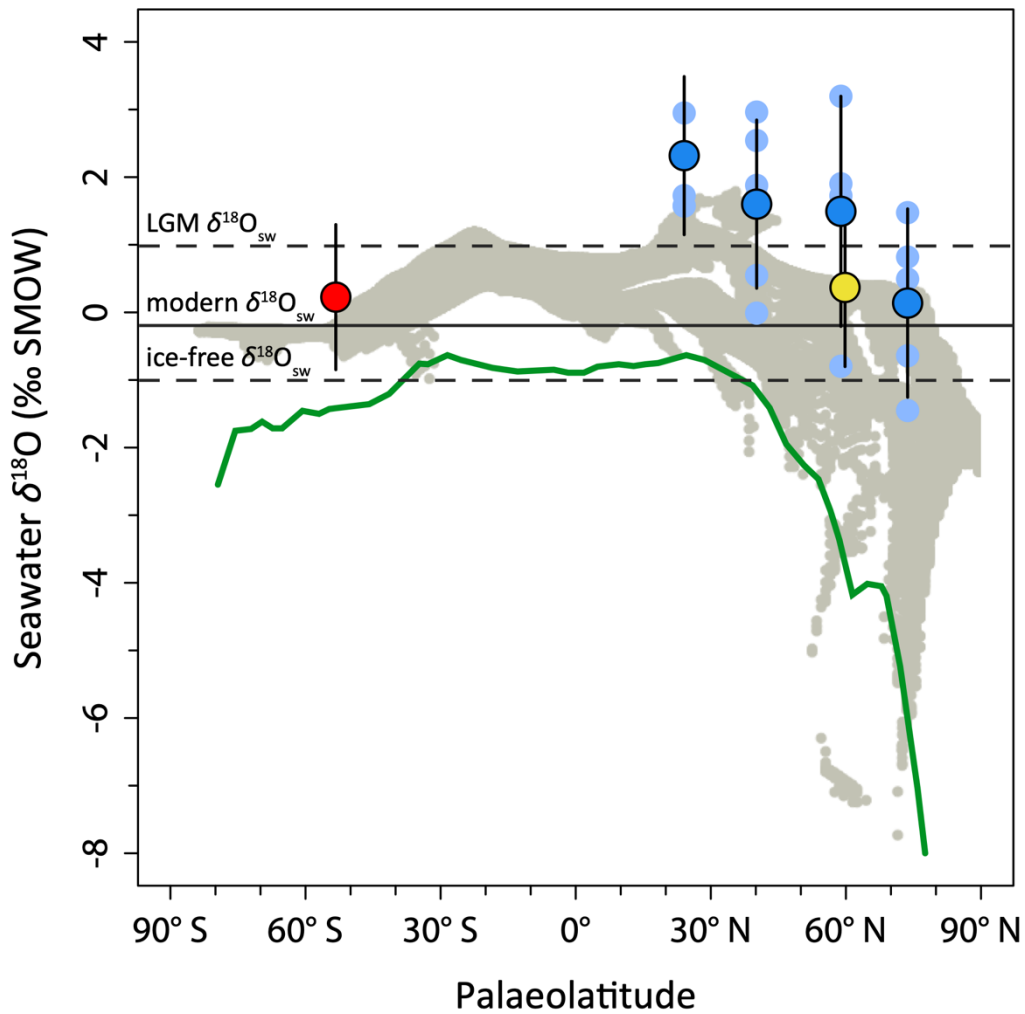
Zonal range of data from the Yatria River

799 **Fig. 2.** Biostratigraphic correlation of the Early Cretaceous Tethyan (Reboulet et al., 2018) sub-
800 Boreal and Boreal (Gradstein et al. 2012; Nunn et al. 2010; Shulgina et al., 1994; Zakharov et al.,
801 1997; Baraboshkin, 2004) ammonite schemes. The green shaded area indicates the position of
802 sampled Valanginian zones for Tethyan (Caravaca, Spain), Sub-Boreal (Speeton), and Boreal
803 sites (Khatanga Basin and Pechora Basin). The ammonite range of additional Valanginian Δ_{47}
804 data from the Yatria River is shown (Price and Passey 2013). Early Cretaceous southern high
805 latitude data shown on Figs 3 and 4 have less constrained biostratigraphy (Vickers et al., 2019).



806 **Fig. 3.** Early Cretaceous (Valanginian) meridional temperature reconstruction. Mean annual
 807 surface temperature observations from the World Ocean Atlas (Locarnini et al., 2013).
 808 Valanginian TEX₈₆ temperatures (Littler et al., 2011) were recalculated using the TEX₈₆^H
 809 calibration (Kim et al., 2010). Dark blue circles show mean Δ_{47} -based temperatures from this
 810 study with \pm uncertainties corresponding to the standard deviation from individual belemnites
 811 (light blue circles). Additional Δ_{47} data of Vickers et al., (2019) (for the Early Cretaceous) and
 812 Price and Passey (2013) (Valanginian) were converted to temperatures using the synthetic
 813 calcite calibration of Petersen et al. (2019). Early Cretaceous data are compared with sea
 814 surface temperatures from the Early Cretaceous (Valanginian) GCM with 4x pre-industrial pCO₂

815 (Lunt et al., 2016) a mid-Cretaceous GCM with 12x pre-industrial $p\text{CO}_2$ (Poulsen et al., 2007) and
816 a Late Cretaceous GCM with 8x pre-industrial $p\text{CO}_2$ (Donnadieu et al., 2016). Thermal gradients
817 of the simulations have been calculated from an average over the longitudes including the
818 South Atlantic sector and the Tethyan area (see Donnadieu et al., 2016). A version of this plot
819 where Δ_{47} -based temperatures are calculated using the Wacker et al. (2014) equation is shown
820 in the Supplementary Information.



821 **Fig. 4.** Early Cretaceous (Valanginian) meridional seawater oxygen isotope gradient. Modern
 822 gridded mean annual $\delta^{18}\text{O}_{\text{sw}}$ values from LeGrande and Schmidt (2006). $\delta^{18}\text{O}_{\text{sw}}$ (‰ SMOW)
 823 calculated using the Kim and O'Neil (1997) equation (see Supplementary Figure 2 for Coplen
 824 (2007) equation) with additional Valanginian data derived from Price and Passey (2013) and
 825 Vickers et al. (2019). Dark blue circles are mean estimates and \pm uncertainties are standard
 826 deviations. Light blue circles are estimates from individual belemnites. Modelled mid
 827 Cretaceous mean annual zonal average of $\delta^{18}\text{O}_{\text{sw}}$ after Zhou, et al. (2008).

828 **Table 1.** Clumped and bulk isotopic composition of Early Cretaceous belemnites

Sample	Taxonomy	Location	N	$\delta^{13}\text{C}$ (‰ VPDB)	$\delta^{18}\text{O}$ (‰ VPDB)	Δ_{47} (RFAC) (‰)	Temperature (°C)	$\delta^{18}\text{O}_{\text{SW}}$ (‰ SMOW) Coplen (2007)	$\delta^{18}\text{O}_{\text{SW}}$ (‰ SMOW) Kim and O'Neil (1997)
KH18-10.50	<i>Acroteuthis</i> sp.	Boyarka	5	0.22	-1.55	0.707 (±0.005)	19 (±1)	-2.1 (±0.3)	-0.6 (±0.3)
KH18-11.20	indet.	Boyarka	5	1.12	-0.48	0.701 (±0.006)	21 (±2)	-0.6 (±0.4)	0.8 (±0.4)
KH18-27.00	<i>Lagonibelus</i> sp.	Boyarka	6	0.96	0.03	0.713 (±0.006)	17 (±2)	-0.9 (±0.4)	0.5 (±0.4)
KH18-2.85	indet.	Boyarka	5	0.38	0.07	0.699 (±0.009)	21 (±3)	0.0 (±0.6)	1.5 (±0.6)
KH18-7.10	<i>Pachyteuthis</i> sp.	Boyarka	5	0.60	-2.19	0.709 (±0.007)	18 (±2)	-2.9 (±0.5)	-1.5 (±0.5)
YCL214-031	<i>Berriasibelus</i> sp.	Caravaca	6	-1.25	-0.57	0.670 (±0.012)	32 (±5)	1.4 (±0.9)	2.9 (±0.9)
YG14-015	<i>Duvalia</i> sp.	Caravaca	3	0.50	0.37	0.671 (±0.007)	31 (±3)	2.3 (±0.5)	3.8 (±0.5)
YP14-005	<i>Hibolithes</i> sp.	Caravaca	5	1.74	-0.41	0.691 (±0.013)	24 (±4)	0.1 (±0.9)	1.6 (±0.9)
YP14-001	<i>Duvalia</i> cf. <i>lata</i>	Caravaca	6	-0.29	-0.50	0.690 (±0.009)	25 (±3)	0.1 (±0.6)	1.6 (±0.7)
YP14-014	<i>Duvalia</i> <i>binervia</i>	Caravaca	4	0.95	-0.27	0.691 (±0.009)	24 (±3)	0.3 (±0.6)	1.7 (±0.6)
PC7-B1	<i>Pachyteuthis</i> sp.	Izhma	7	-0.49	0.21	0.735 (±0.004)	10 (±1)	-2.1 (±0.3)	-0.8 (±0.3)
PC7-B2	<i>Pachyteuthis</i> sp.	Izhma	6	0.19	0.56	0.700 (±0.003)	21 (±1)	0.5 (±0.2)	1.9 (±0.2)

PC9-G23	indet.	Izhma	5	-0.79	0.52	0.702 (±0.007)	20 (±2)	0.3 (±0.5)	1.7 (±0.5)
PC9-G8	<i>Acroteuthis</i> sp.	Izhma	7	1.16	0.98	0.688 (±0.005)	25 (±2)	1.7 (±0.3)	3.2 (±0.3)
D2E	<i>Acroteuthis</i> sp.	Speeton	2	-0.46	-0.36	0.690 (±0.007)	25 (±2)	0.3 (±0.5)	1.7 (±0.5)
D3D	<i>Acroteuthis</i> sp.	Speeton	2	-0.09	-0.21	0.680 (±0.020)	28 (±7)	1.1 (±1.4)	2.5 (±1.4)
D4A	<i>Acroteuthis</i> sp.	Speeton	6	0.51	0.41	0.683 (±0.004)	27 (±1)	1.5 (±0.3)	3.0 (±0.3)
SP 1181	<i>Acroteuthis</i> sp.	Speeton	5	-0.12	-0.60	0.711 (±0.004)	18 (±1)	-1.4 (±0.3)	0.0 (±0.3)
SP 1297	<i>Acroteuthis</i> sp.	Speeton	4	0.60	-0.89	0.699 (±0.005)	22 (±2)	-0.9 (±0.3)	0.5 (±0.3)
SP 1S22C	<i>Acroteuthis</i> sp.	Speeton	5	0.60	-0.36	0.688 (±0.005)	25 (±2)	0.4 (±0.3)	1.9 (±0.3)

829 The standard error of the carbonate $\delta^{13}\text{C}$ and $\delta^{18}\text{O}$ values is 0.01‰. The \pm uncertainty in the
830 Δ_{47} (RFAC) values represents the (external) standard error of 2–7 replicate analyses, multiplied by
831 the t -value that corresponds to the number of replicates (68.2% confidence interval). The
832 Δ_{47} (RFAC) values were converted to temperatures using synthetic calcite calibration (Petersen et
833 al., 2019) as discussed in the text (Data S1). The error in the calculated temperatures and $\delta^{18}\text{O}_{\text{sw}}$
834 correspond to the standard error of the Δ_{47} (RFAC) values.

835 **Table 2.** Mean seawater temperatures and $\delta^{18}\text{O}_{\text{sw}}$ for the locations in this study.

Location	Palaeolatitude	Number of belemnites	Mean seawater temperature (°C)	Mean $\delta^{18}\text{O}_{\text{sw}}$ (‰ SMOW) Coplen (2007)	Mean $\delta^{18}\text{O}_{\text{sw}}$ (‰ SMOW) Kim and O'Neil (1997)
Caravaca	24° N	5	27 (±4)	0.8 (±1.1)	2.3 (±1.2)
Speeton	40° N	6	24 (±4)	0.1 (±1.2)	1.6 (±1.2)
Izhma	59° N	4	19 (±7)	0.1 (±1.7)	1.5 (±1.7)
Boyarka	74° N	5	19 (±2)	-1.3 (±1.4)	0.1 (±1.4)

836 The ± uncertainties for the mean temperatures are calculated using the standard deviation of
 837 the $\Delta_{47}(\text{RFAC})$ values of the individual belemnites (Table 1). This uncertainty was combined with
 838 the standard deviation of the $\delta^{18}\text{O}$ values of the individual belemnites to calculate the ±
 839 uncertainties for the mean $\delta^{18}\text{O}_{\text{sw}}$ values. Palaeolatitude estimates are from Young et al. (2019).